the superposition of electronic states in long conjugated molecules contributes to large second-order hyperpolarizabilities is worthy of further investigation.

While these conclusions apply strictly to the acetylene-linked donor–acceptor pairs investigated here, a comparison to other donor–acceptor molecules indicates that many of these observations may be general. A recent study of donor–acceptor benzene and stilbene compounds indicates that, within a series, the value of β is dominated by the energy of the ICT transition.[3a] In comparing totally different molecules it is clear that other factors, such as dipole moment change and transition moment, play a significant role. In general, the donor–acceptor benzenes had smaller values of β than either the stilbene or acetylene derivatives for similar ICT band energies. Furthermore, the stilbene-linked donor–acceptor pairs have larger β values than the acetylene linkers. This is due to the greater degree of conjugation inherent in the ethylene-linked π system. The acetylene group, which possesses a short carbon–carbon bond (a constraint imposed by the in-plane π bond), does not overlap as well with the π system on the phenyl groups as the ethylene bridge. This is reflected in the position of the ICT band which is at lower energy for the stilbene than for the acetylene linker (402 vs 381 nm respectively for the amino–nitro donor–acceptor pair). Likewise the β value is larger for the stilbene than the acetylene (24×10^{-30} vs 40×10^{-30} esu, respectively, for the amino–nitro derivatives). It is worth noting than the very large value of β observed for the amino–nitro stilbene relative to the diphenylacetylene analogue is due not only to the lower ICT transition energy but also to a larger dipole moment change; this suggests that factors such as $\Delta\mu$ are more important in going from one class of molecules to another and that they are within a homologous series.

Acknowledgment. This work was performed in part by the Jet Propulsion Laboratory, California Institute of Technology, as part of its Center for Space Microelectronics Technology, which is supported by the Strategic Defense Initiative Organization, Innovative Science and Technology Office through an agreement with the National Aeronautics and Space Administration.

Structure and Mesophases of Hexacyclen Derivatives

Stefan H. J. Idziak,[†] Nicholas C. Maliszewskyj,[†] Paul A. Heiney,*[,†] John P. McCauley, Jr.,[‡] Paul A. Sprengeler,[‡] and Amos B. Smith, III*[,‡]

Contribution from the Departments of Chemistry and Physics, and Laboratory for Research on the Structure of Matter, University of Pennsylvania, Philadelphia, Pennsylvania 19104.
Received March 28, 1991.

Abstract: A variety of hexacyclen derivatives with aliphatic substituents have been prepared and characterized via X-ray diffraction, calorimetry, thermogravimetric analysis, and computer simulations. A subset of these compounds (**2a** and **2e**) are seen to display a liquid crystalline mesophase, while others transform directly from the crystalline to the isotropic liquid phase. The merits of tubular and smectic liquid crystalline models for the mesophase structure are discussed.

1. Introduction

It is generally considered that the liquid crystalline phases formed by a mesogenic compound are primarily determined by the geometry of the constituent molecules; traditional prolate molecules form layered smectic phases or nematic phases, while highly oblate "discotic" molecules[1,2] form columnar or discotic nematic phases. Although the majority of discogenic molecules studied have flat, rigid cores with six or more flexible aliphatic tails, columnar-phase formation is possible with a remarkable degree of molecular nonplanarity and asymmetry.[2] Accordingly, when Lehn et al. found[3] that the hexakis(*p*-(*n*-dodecyloxy)benzoyl) derivative of hexasubstituted azacrown[18]-N_6 (**2a**) (Scheme I) exhibited mesogenic behavior, the most natural hypothesis was that a columnar structure was formed. This hypothesis was strengthened by microscopic and X-ray observations of samples oriented by shearing or slow cooling on a glass substrate. Furthermore, the structural representation in Scheme I exhibits an intriguing, albeit small, open space in the center of the molecule, leading to the description of the mesophase structure as "tubular": consisting of a hexagonal disordered columnar phase ("D_{hd}") with *hollow* columns.

Several subsequent studies of **2a** and related compounds[4-7] were essentially consistent with those of Lehn et al., although phase-transition temperatures were found to vary from laboratory to laboratory. It has been suggested[6] that these variations arise from differing amounts of water in the highly hygroscopic samples. It is also seen that mesophase formation is quite sensitive to tail structure;[5] in particular, only substituents consisting of proximal aromatic residues with aliphatic tails result in mesophase formation.

Scheme I

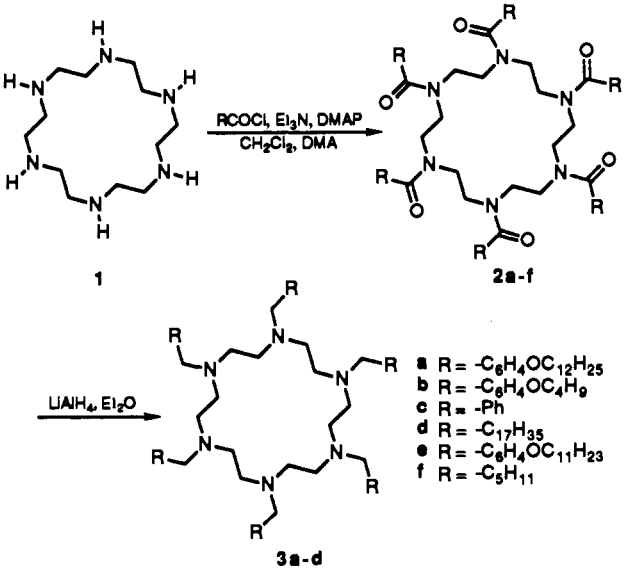

[†] Department of Physics.
[‡] Department of Chemistry.

(1) Chandrasekhar, S.; Sadashiva, B. K.; Suresh, K. *Pramana* **1977**, *9*, 471.
(2) Chandrasekhar, S.; Ranganath, G. S. *Rep. Prog. Phys.* **1990**, *53*, 57–84.
(3) Lehn, J. M.; Malthete, J.; Levelut, A. M. *J. Chem. Soc., Chem. Commun.* **1985**, 1794–1796.

0002-7863/91/1513-7666$02.50/0

In this paper, we describe the synthesis of nine derivatives of hexasubstituted azacrown[18]-N_6 and their characterization via X-ray diffraction, differential scanning calorimetry (DSC), thermogravimetric analysis (TGA), and optical microscopy. These measurements, and in particular the X-ray diffraction results, led us to conclude that the data are described at least as well by a smectic arrangement of linear molecules as by a columnar arrangement of tubular molecules. Computer simulations provide additional insight into the most likely conformations of the isolated [18]-N_6 derivatives.

2. Synthesis

Derivatives of 1,4,7,10,13,16-hexaazacyclooctadecane (**1**, [18]-N_6) were synthesized to explore the possibilities of mesophase formation (Scheme I). The nitrogen analogue of 18-crown-6 was prepared according to the method of Atkins, Richman, and Oettle.[8] This cyclic amine was then acylated by treatment with a series of acyl chlorides in the presence of triethylamine, in a manner analogous to that reported by Lehn and co-workers,[3] to furnish cyclic hexamides **2a–f**, differing in side-chain substitution. A second series was prepared by reduction of the amide functionalities with lithium aluminum hydride to provide either cyclic alkyl- or benzyl-substituted tertiary amines **3a–d**. Complete experimental procedures and physical data for each compound are presented in the Experimental Section.

Experimental Section

Materials and Methods. All reactions were performed under an argon atmosphere with oven-dried glassware. Diethyl ether was distilled from sodium benzophenone ketyl. Triethylamine and methylene chloride were distilled from calcium hydride. Lithium aluminum hydride was purchased from Aldrich as a 1.0 M solution in diethyl ether. Anhydrous *N,N*-dimethylacetamide, (dimethylamino)pyridine, benzoyl chloride, and hexanoyl chloride were obtained from Aldrich and used without further purification; other acid chlorides were prepared from the corresponding carboxylic acids by treatment with thionyl chloride. 1,4,7,10,13,16-Hexaazacyclooctadecane (**1**, [18]-N_6) was prepared according to the method of Atkins, Richman, and Oettle.[8]

Silica gel, particle size 0.040–0.063 mm, supplied by E. Merck, was used for flash chromatography. Neutral alumina, Brockman activity 1 (80–200 mesh), was purchased from Fisher Scientific. Anhydrous Na_2SO_4 and K_2CO_3 were obtained from EM Sci.

Proton and carbon NMR spectra were recorded on a Bruker AM 500 spectrometer in $CDCl_3$ at 300 K unless otherwise indicated. Chemical shifts are reported in δ values in ppm relative to tetramethylsilane (δ = 0) for proton NMR and relative to chloroform-*d* (δ = 77.0) for the carbon NMR spectra. Chemical shifts are reported relative to characteristic solvent absorbances in elevated temperature experiments (C_6D_6, δ = 7.15, $C_6D_5CD_3$ δ = 2.09 for proton NMR and C_6D_6 δ = 128.0, $C_6D_5CD_3$ δ = 20.4, DMSO-d_6 δ = 39.5 for carbon NMR). Coupling constants are reported in hertz. Infrared spectra were recorded on a Perkin-Elmer Model 283B spectrophotometer as $CHCl_3$ solutions. High-resolution mass spectra were recorded by Mr. John Dykins of the University of Pennsylvania Mass Spectrometry Center.

General Procedure for Acylation of [18]-N_6 (1) with Acyl Halides. A three-neck 250-mL round-bottom flask equipped with an addition funnel, reflux condenser, argon balloon, and magnetic stirrer was charged with 1.00 g (3.86 mmol, 1.0 equiv) of the cyclic hexaamine **1**, 5.0 mL (68 mmol, 17.6 equiv) of triethylamine, and 47 mg (0.38 mmol, 0.1 equiv) of (dimethylamino)pyridine. This material was dissolved in 25 mL of dry *N,N*-dimethylacetamide and then diluted with 50 mL of CH_2Cl_2. The reaction vessel was then cooled to 0 °C, and the acid chloride (25.5 mmol, 6.6 equiv) was added dropwise over 1 h as a solution in 75 mL CH_2Cl_2. After the addition was complete, the mixture was allowed to warm to room temperature and then heated to reflux for 36 h. At the end of this period, the mixture was allowed to cool and was then quenched with 75 mL of saturated NH_4Cl solution. The aqueous layer was extracted two times with 50 mL of $CHCl_3$, and the combined organic extracts were washed with 50 mL of saturated $NaHCO_3$, 100 mL of water (two times), and 50 mL of brine, and then dried over anhydrous Na_2SO_4. Filtration and then concentration on a rotary evaporator followed by silica gel flash chromatography employing 3% $CH_3OH/CHCl_3$ as eluent provided cyclic hexaamides **2a–f**. Further purification was achieved by recrystallization from the designated solvent and drying in vacuo.

1,4,7,10,13,16-Hexakis(4-(dodecyloxy)benzoyl)-1,4,7,10,13,16-hexaazacyclooctadecane (2a).[3] Recrystallized from CH_2Cl_2/CH_3OH (83% yield): IR ($CHCl_3$) 3002 (m), 2937 (s), 2865 (s), 1628 (s), 1616 (s), 1465 (s), 1425 (s), 1249 (s), 1175 (s), 838 (m) cm^{-1}; ^1H NMR (500 MHz, C_6D_6, 350 K) δ 0.92 (t, J = 6.9 Hz, 18 H), 1.23–1.34 (m, 96 H), 1.34–1.38 (m, 12 H), 1.61–1.67 (m, 12 H), 3.73 (t, J = 6.5 Hz, 12 H), 3.82 (s, 24 H), 6.86 (d, J = 8.6 Hz, 12 H), 7.50 (d, J = 8.6 Hz, 12 H); ^{13}C NMR (125 MHz, C_6D_6, 350 K) δ 14.10, 22.97, 26.40, 29.64, 29.69, 29.76, 29.94, 30.01, 30.04, 32.26, 48.54 (br), 68.43, 114.89, 128.69, 129.71, 161.17, 172.14; high-resolution mass spectrum (FAB) m/z 1989.5312 [$(M + H)^+$, calcd for $C_{126}H_{199}N_6O_{12}$ 1989.5146].

1,4,7,10,13,16-Hexakis(4-(butyloxy)benzoyl)-1,4,7,10,13,16-hexaazacyclooctadecane (2b). Recrystallized from CH_2Cl_2/hexanes (83% yield): IR ($CHCl_3$) 3007 (m), 2970 (s), 2881 (m), 1630 (s), 1615 (s), 1512 (m), 1468 (s), 1426 (s), 1305 (s), 1253 (s), 1177 (s), 839 (m) cm^{-1}; ^1H NMR (500 MHz, C_6D_6, 350 K) δ 0.81 (t, J = 7.3 Hz, 18 H), 1.26–1.34 (m, 12 H), 1.51–1.57 (m, 12 H), 3.67 (t, J = 6.4 Hz, 12 H), 3.84 (s, 24 H), 6.81 (d, J = 8.5 Hz, 12 H), 7.45 (d, J = 8.5 Hz, 12 H); ^{13}C NMR (125 MHz, DMSO-d_6, 420 K) δ 12.28, 17.70, 30.00, 45.99, 67.25, 113.84, 127.57, 127.59, 159.16, 170.17; high-resolution mass spectrum (FAB) m/z 1315.7519 [$(M + H)^+$, calcd for $C_{78}H_{103}N_6O_{12}$ 1315.7634].

1,4,7,10,13,16-Hexabenzoyl-1,4,7,10,13,16-hexaazacyclooctadecane (2c).[9] Recrystallized from CH_2Cl_2/EtOAc (89% yield): IR ($CHCl_3$) 2985 (s), 1630 (s), 1415 (s), 1267 (s), 1123 (s) cm^{-1}; ^1H NMR (500 MHz, C_6D_6, 350 K) δ 3.65 (s, 24 H), 7.05–7.12 (m, 18 H), 7.30 (br s, 12 H); ^{13}C NMR (125 MHz, $C_6D_5CD_3$, 380 K) δ 48.31, 127.73, 129.97, 137.00, 172.26; high-resolution mass spectrum (FAB) m/z 883.4255 [$(M + H)^+$, calcd for $C_{54}H_{55}N_6O_6$ 883.4183].

1,4,7,10,13,16-Hexaoctadecanoyl-1,4,7,10,13,16-hexaazacyclooctadecane (2d). Recrystallized from $CHCl_3/CH_3OH$ (37% yield): IR ($CHCl_3$) 2938 (s), 2880 (s), 1643 (s), 1465 (s), 1420 (m), 1179 (m) cm^{-1}; ^1H NMR (500 MHz, $C_6D_5CD_3$, 380 K) δ 0.92 (t, J = 6.8 Hz, 18 H), 1.27–1.53 (m, 168 H), 1.76–1.84 (m, 12 H), 2.34–2.61 (br s, 12 H), 3.39 (br s, 24 H); ^{13}C NMR (125 MHz, $C_6D_5CD_3$, 380 K) δ 14.16, 23.15, 26.15, 29.93, 30.17, 30.28, 30.37, 32.52, 33.59, 47.98 (br), 174.02 (br); high-resolution mass spectrum (FAB) m/z 1856.8380 [$(M + H)^+$, calcd for $C_{120}H_{235}N_6O_6$ 1856.8190].

1,4,7,10,13,16-Hexakis(4-(undecyloxy)benzoyl)-1,4,7,10,13,16-hexaazacyclooctadecane (2e). Recrystallized from $CHCl_3/CH_3OH$ (85% yield): IR ($CHCl_3$) 3001 (m), 2940 (s), 2868 (s), 1639 (s), 1611 (s), 1511 (m), 1462 (s), 1427 (s), 1305 (s), 1251 (s), 1177 (s), 838 (m) cm^{-1}; ^1H NMR (500 MHz, $C_6D_5CD_3$, 380 K) δ 0.88 (t, J = 6.8 Hz, 18 H), 1.21–1.35 (m, 84 H), 1.35–1.40 (m, 12 H), 1.58–1.67 (m, 12 H), 3.74 (s, 24 H), 3.76 (t, J = 6.5 Hz, 12 H), 6.79 (d, J = 8.6 Hz, 12 H), 7.39 (d, J = 8.6 Hz, 12 H); ^{13}C NMR (125 MHz, $C_6D_5CD_3$, 380 K) δ 14.16, 19.94, 20.86, 23.13, 26.72, 29.88, 30.02, 30.20, 32.49, 48.81, 68.96, 115.31, 129.88, 161.47, 172.27; high-resolution mass spectrum (FAB) m/z 1904.4441 [$(M + H)^+$, calcd for $C_{120}H_{187}N_6O_{12}$ 1904.4207].

1,4,7,10,13,16-Hexahexanoyl-1,4,7,10,13,16-hexaazacyclooctadecane (2f). Recrystallized from CH_3OH/H_2O (89% yield): IR ($CHCl_3$) 2998 (s), 2975 (s), 2941 (s), 2877 (s), 1645 (s), 1456 (s), 1421 (s), 1382 (m), 1244 (m), 1179 (s), 1111 (m) cm^{-1}; ^1H NMR (500 MHz, $C_6D_5CD_3$, 380 K) δ 0.89 (t, J = 6.9 Hz, 18 H), 1.26–1.41 (m, 24 H), 1.66–1.77 (m, 12 H), 2.25–2.52 (br s, 12 H), 3.32 (br s, 24 H); ^{13}C NMR (125 MHz, $C_6D_5CD_3$, 380 K) δ 14.03, 22.94, 25.69, 32.33, 33.48, 47.86 (br), 174.00 (br); high-resolution mass spectrum (FAB) m/z 847.7093 [$(M + H)^+$, calcd for $C_{48}H_{91}N_6O_6$ 847.7001].

General Procedure for Reduction of Hexaamides 2a–d. A three-neck 100-mL round-bottom flask fitted with an efficient reflux condenser, magnetic stirrer, and argon balloon was charged with 1.15 mmol (1.0 equiv) of the cyclic hexaamide **2** and 50 mL of dry diethyl ether. The solution was cooled to 0 °C, and 9.0 mL of a 1.0 M solution of lithium aluminum hydride in diethyl ether (9.0 mmol, 7.8 equiv) was added slowly via syringe. After the addition was complete, the reaction mixture was heated to reflux for 36 h. At the end of this period, the mixture was cooled and the reaction cautiously quenched via sequential addition of 0.34 mL of water, 0.34 mL of 15% NaOH solution, and 1.03 mL of water. The resultant aluminum salts were removed by filtration, and the precipitate was washed with diethyl ether and methylene chloride. The combined organic extracts were then dried over anhydrous K_2CO_3 fol-

(4) Lattermann, G. *Mol. Cryst. Liq. Cryst.* **1990**, *182B*, 299–311.
(5) Mertesdorf, C.; Ringsdorf, H. *Liq. Cryst.* **1989**, *5*, 1757–1772.
(6) Tatarsky, D.; Banerjee, K.; Ford, W. T. *Chem. Mater.* **1990**, *2*, 138–141. *Polym. Prepr.* **1989**, *30(2)*, 460–461.
(7) Malthete, J.; Poupinet, D.; Vilanove, R.; Lehn, J. M. *J. Chem. Soc., Chem. Commun.* **1989**, 1016–1019.
(8) Atkins, T. J.; Richman, J. E.; Oettle, W. F. *Org. Synth.* **1978**, *58*, 86–98.
(9) Tsukube, H.; Takagi, K.; Higashiyama, T.; Iwachido, T.; Hayama, N. *J. Chem. Soc., Perkin Trans. 2* **1985**, 1541–1545.

lowed by filtration through a plug of neutral alumina with ether and methylene chloride as the eluent. The solvent was then removed in vacuo to give the cyclic tertiary hexaamine **3**. Recrystallization from the designated solvent and drying in vacuo provided the pure amine **3**.

1,4,7,10,13,16-Hexakis(4-(dodecyloxy)benzyl)-1,4,7,10,13,16-hexaazacyclooctadecane (3a). Recrystallized from CH_2Cl_2/CH_3OH (49% yield): IR ($CHCl_3$) 2940 (s), 2872 (s), 1610 (m), 1513 (s), 1467 (m), 1245 (s) cm^{-1}; ^1H NMR (500 MHz, $CDCl_3$) δ 0.88 (t, J = 6.9 Hz, 18 H), 1.21–1.39 (m, 96 H), 1.39–1.51 (m, 12 H), 1.71–1.82 (m, 12 H), 2.57 (s, 24 H), 3.38 (s, 12 H), 3.91 (t, J = 6.6 Hz, 12 H), 6.76 (d, J = 8.5 Hz, 12 H), 7.05 (d, J = 8.5 Hz, 12 H); ^{13}C NMR (125 MHz, $CDCl_3$) δ 14.10, 22.68, 26.11, 29.35, 29.47, 29.63, 29.68, 31.92, 52.19, 58.60, 67.98, 114.07, 129.91, 131.40, 158.03; high-resolution mass spectrum (FAB) m/z 1904.6113 [(M + H)$^+$, calcd for $C_{126}H_{211}N_6O_6$ 1904.6390].

1,4,7,10,13,16-Hexakis(4-(butyloxy)benzyl)-1,4,7,10,13,16-hexaazacyclooctadecane (3b). Recrystallized from Et_2O/CH_3OH (75% yield): IR ($CHCl_3$) 2969 (s), 2880 (s), 1606 (m), 1512 (s), 1468 (m), 1145 (s) cm^{-1}; ^1H NMR (500 MHz, $CDCl_3$) δ 0.97 (t, J = 7.4 Hz, 18 H), 1.41–1.52 (m, 12 H), 1.71–1.80 (m, 12 H), 2.58 (s, 24 H), 3.38 (s, 12 H), 3.93 (t, J = 6.5 Hz, 12 H), 6.77 (d, J = 8.6 Hz, 12 H), 7.05 (d, J = 8.6 Hz, 12 H); ^{13}C NMR (125 MHz, $CDCl_3$) δ 13.87, 19.27, 31.43, 52.20, 58.59, 67.64, 114.06, 129.92, 131.41, 158.03; high-resolution mass spectrum (FAB) m/z 1231.8801 [(M + H)$^+$, calcd for $C_{78}H_{115}N_6O_6$ 1231.8878].

1,4,7,10,13,16-Hexabenzyl-1,4,7,10,13,16-hexaazacyclooctadecane (3c).[10] Recrystallized from CH_2Cl_2/CH_3OH (52% yield): IR ($CHCl_3$) 3070 (m), 3006 (m), 2958 (s), 2810 (s), 1905 (w), 1870 (w), 1815 (w), 1601 (m), 1498 (s), 1455 (s), 1369 (s), 1101 (s), 690 (s) cm^{-1}; ^1H NMR (500 MHz, $CDCl_3$) δ 2.62 (s, 24 H), 3.45 (s, 12 H), 7.16–7.24 (m, 30 H); ^{13}C NMR (125 MHz, $CDCl_3$) δ 52.42, 59.30, 126.69, 128.06, 128.78, 139.64; high-resolution mass spectrum (FAB) m/z 799.5333 [(M + H)$^+$, calcd for $C_{54}H_{67}N_6$ 799.5427].

1,4,7,10,13,16-Hexaoctadecyl-1,4,7,10,13,16-hexaazacyclooctadecane (3d). Recrystallized from $CHCl_3/CH_3OH$ (15% yield): IR ($CHCl_3$) 2942 (s), 2873 (s), 1476 (m), 1091 (m) cm^{-1}; ^1H NMR (500 MHz, $CDCl_3$) δ 0.88 (t, J = 6.9 Hz, 18 H), 1.19–1.36 (m, 180 H), 1.38–1.48 (m, 12 H), 2.42 (t, J = 7.4 Hz, 12 H), 2.55 (s, 24 H); ^{13}C NMR (125 MHz, $CDCl_3$) δ 14.09, 22.68, 27.41, 27.57, 29.36, 29.67, 29.72, 31.93, 52.93, 55.70; high-resolution mass spectrum (FAB) m/z 1772.9731 [(M + H)$^+$, calcd for $C_{120}H_{247}N_6$ 1772.9512].

3. Physical Characterization

Low-resolution X-ray powder measurements were performed as described previously.[11,12] We used Cu Kα radiation from a rotating-anode generator, a focussing LiF monochromator crystal, a flat LiF analyzer crystal, and a scintillation detector to obtain an instrumental resolution Δq = 0.007 Å^{-1} full-width at half-maximum (FWHM). (We use the convention $q \equiv 2\pi/d = 4\pi/\lambda \sin\theta$.) For one sample, additional high-resolution X-ray diffraction results were obtained by using synchrotron radiation at the National Synchrotron Light Source (NSLS). In this case, we used the sagitally focussed Si monochromator crystal at beam line X9A together with a flat Ge analyzer crystal to obtain a resolution of 0.0008 Å^{-1} FWHM.

For X-ray measurements, the samples were placed in 1.0-mm glass capillary tubes with 0.01-mm wall thickness. Each capillary was loaded (in air) by repeatedly packing the tube with powder at room temperature and then heating into the isotropic phase. Flow of the liquid to the bottom of the tube was enhanced by the insertion of a clean wire. The tube was then mounted in a brass sample holder and placed in an X-ray oven with a ±0.1 °C temperature control. Measurements were performed on cooling from at least 10 °C above the isotropic transition temperature to about 60 °C over 24 h. At each temperature, the diffracted intensity was typically measured between q = 0.05 Å^{-1} and 2.5 Å^{-1}. Finally, each sample was cooled to room temperature and allowed to sit for 1 week before a room temperature powder diffractogram was measured.

Differential scanning calorimetry (DSC) measurements were performed with a Du Pont 910 cell and a Du Pont 2100 thermal analyzer. Samples were loaded into pans without tops to minimize surface effects. The samples were heated 5 °C/min from room temperature to about 180 °C under nitrogen. In cases where interesting thermal behavior was observed or expected from other measurements, the sample was then cooled and the DSC heating scan was repeated. In some cases, this resulted in thermal behavior different from the first heating cycle, but third and successive heating measurements, when performed, were always in agreement with the second heating cycle. Unless otherwise stated, quoted temperatures derived from DSC measurements are those taken from the second heating.

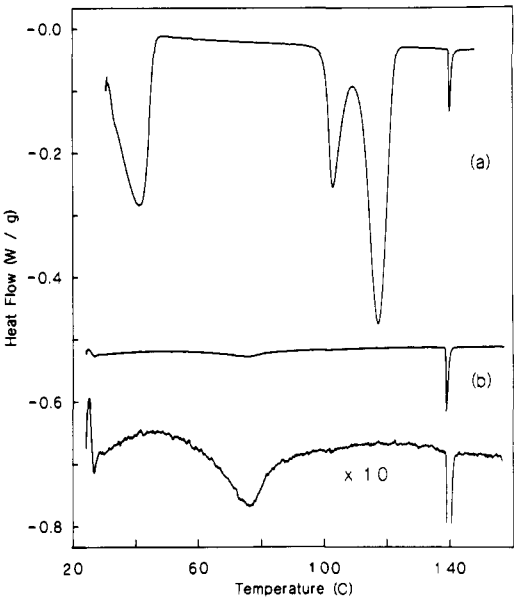

Figure 1. Differential scanning calorimetry curves for **2a**. The scan for the as-prepared sample is shown in (a). The initial broad peak is probably due to solvents evolving from the sample. The enthalpies for the peaks at 103 and 118 °C are 7.0 and 17.4 kcal/mol, respectively. The peak at 140 °C corresponds to the transition to the isotropic phase. The curve for second heating is given in (b) with the same curve magnified 10 times to enlarge the feature at 75 °C that is discussed in the text.

Thermogravimetric analysis (TGA) was done on a Du Pont 951 TGA with a VG Micromass 300D mass spectrometer. Samples were heated 10 °C/min under nitrogen from room temperature to 250 °C. Optical microscopy studies were done with a Reichert microscope equipped with a Mettler FP52 heating stage.

4. Samples Displaying Mesogenic Behavior

The samples studied are given in Scheme I. The only compounds that we studied that were observed to display a liquid crystal phase were **2a** (the compound originally studied by Lehn et al.)[3] and **2e**. DSC curves for the first two heating cycles of **2a** are shown in Figure 1. Crystal to mesophase and mesophase to isotropic phase transition temperatures were determined to be 64 and 140 °C on the second DSC heating cycle. As can be seen from the figure, the second DSC heating cycle for **2a** is quite different from the first. Following the suggestion of Tatarsky et al.[6] that phase-transition temperatures in these compounds are strongly dependent on residual solvent and water present in the samples, we performed TGA measurements and examined the evolution of water, methanol, and CH_2Cl_2. We found that the peak centered on 45 °C in the first heating is due to water evolving from the sample; methanol or CH_2Cl_2 were not present in the sample. We believe the differences between the peaks at 76, 103, and 118 °C are due to surface-pinning effects on the DSC sample cell. The extremely broad peak at 76 °C indicates that the transition occurs very slowly and that there is some form of equilibrium between two states over a large temperature range; perhaps the transition is characterized by a change in conformation of the molecule, which results in a small structure change in the crystal. This broad peak is completely reproducible, even if the

(10) Tsukube, H. *J. Chem. Soc., Perkin Trans. 1* **1985**, 615–619.
(11) Heiney, P. A.; Fontes, E.; de Jeu, W. H.; Riera, A.; Carroll, P.; Smith, A. B., III *J. Phys. (Paris)* **1989**, *50*, 461–483.
(12) Lee, W. K.; Wintner, B. A.; Fontes, E.; Heiney, P. A.; Ohba, M.; Haseltine, J. N.; Smith, A. B., III *Liq. Cryst.* **1989**, *4*, 87–102.

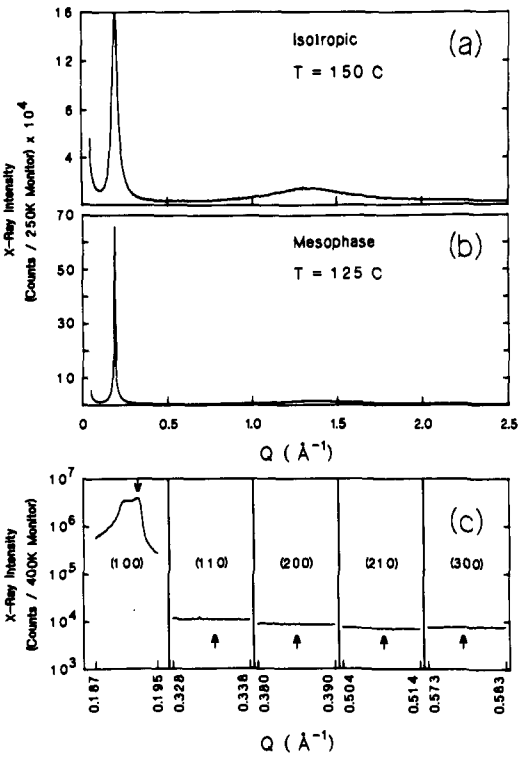

Figure 2. X-ray diffractograms of **2a** powder samples. (a) and (b) were measured on a rotating-anode diffractometer. Each point was counted for 80 s and the point spacing is 0.003 Å^{-1}. The peak centered at 0.1925 Å^{-1} arises from highly developed molecular correlations with a d spacing of 32.6 Å. The broad peak at 1.4 Å^{-1} most likely arises from short-range correlations between paraffinic tails. Patterns in (c) were measured at NSLS beamline X9A; the lowest order (100) peak and the scattering near the positions of the (110), (200), (210), and (300) peaks calculated from a hexagonal columnar lattice are shown in an expanded scale. Each point was counted for approximately 75 s (scaled to beam flux) and the point spacing is 0.0002 Å^{-1}. Arrows indicate the expected positions of the peaks, of which only the (100) is visible. The double peak seen is due to the mosaic of our sample; a perfect powder would only yield a single peak.

sample has been slowly cooled to room temperature over 11 h.

The DSC-determined temperatures correspond with our low-resolution powder X-ray diffraction results, which indicate transitions at 97 ± 5 and 141 ± 5 °C. Typical diffractograms are shown in Figure 2. The diffraction pattern in the isotropic phase is typical of such patterns in both smectogenic and discogenic liquid crystal compounds, indicating short-range correlations at two characteristic distances. The diffuse peak at low q arises from a relatively large nearest-neighbor distance of ~32 Å, while the broad peak at 1.4 Å^{-1} is almost certainly due to the ~4.5 Å closest approach distance of paraffinic tails. As the sample is cooled to the mesophase, the low-q peak sharpens considerably to become resolution-limited, while the broad high-q peak remains essentially unchanged. At room temperature, a number of sharp peaks are observed in addition to a persistent diffuse maximum near 1.4 Å^{-1}. This almost certainly indicates a three-dimensional crystal structure with considerable short-range disorder; however, the detailed structure of the crystal phase has not been determined. The broad peak observed in the DSC for this transition suggests that the crystal phase is closely related to the mesophase.

The diffraction in the mesophase was further characterized by high-resolution powder diffraction experiments at the National Synchrotron Light Source. The position of the low-q peak, which we identify as the (100) Bragg peak of an as yet unknown structure, was 0.1925 Å^{-1}. Even in the high-resolution measurements, the peak was resolution-limited to 0.0008 Å^{-1} FWHM, implying a correlation length larger than 7800 Å. There is evidently long-range order in at least one dimension. Following the hypothesis that the mesophase corresponds to a hexagonal columnar structure, we made detailed measurements in the region of the expected (110), (200), (210), and (300) hexagonal peaks as shown in Figure 2. None of these peaks was observed; taking into account the magnitude of the background scattering and our counting statistics, we can state that these peaks must be reduced in intensity by a factor of at least 5000 from the primary (100) diffraction peak. (Note that if the structure were rectangular-columnar rather than hexagonal-columnar, the positions of the (110) and (210) peaks would be shifted, but the (200) and (300) peaks would still be at the positions we measured.) By contrast, in a typical triphenylene derivative discotic liquid crystal, the ratios of these higher order peak intensities to that of the (100) are 1:220, 1:253, 1:16000, and 1:9000, respectively.[11] The implications of this comparison for the columnar model will be discussed at the end of the paper; we simply note here that lack of higher order diffraction peaks is characteristic of smectic phases.

We made several attempts to prepare aligned samples for a more detailed structural study. We first attempted to prepare single-orientation strands via the pin-and-cup technique.[11,13,14] When successful, this technique results in columns aligned along the strand axis and a small number of hexagonal domains. Unfortunately, strands of **2a** drawn in the mesophase were not self-supporting; if the strands were pulled quickly (ca. 2 mm/min), an hourglass-shaped strand was formed, which thinned at the center and broke after a few minutes. The strands would also break while being pulled if a more reasonable speed of 2 mm/18 h was used. It *was* possible to cool a sample from the isotropic phase through the mesophase down to 90 °C, below the nominal crystal-formation temperature, and then pull a strand at this temperature. This indicates that it is possible to supercool the mesophase under certain conditions, perhaps leading to a liquid crystal glass. However, X-ray studies revealed that there was no preferred orientation in the resultant strand. Also, unlike our previous studies of columnar mesophases,[11,14] the strands were more stable when drawn quickly rather than slowly.

We also studied the effect of surfaces and magnetic fields on sample alignment. A sample of **2a** was loaded in a 0.5-mm capillary tube and placed in an optional 3-kG magnetic field.[15] It was heated to the isotropic phase and then slowly cooled into the mesophase. The orientation was then tested by using X-ray diffraction. It was found that the magnetic field per se had no discernible effect on the alignment, but that the use of a 0.5-mm capillary tube instead of a 1-mm tube induced considerable orientation. The intensity of the sharp low-q peak was considerably stronger when the scattering wave vector was normal to the long axis of the tube. In the 0.5-mm tube, the intensity of this peak was 8 times less with the scattering vector oriented 45° from the tube axis than with it perpendicular to the tube axis. The same intensity only changed by a factor of 2 in the 1-mm capillary tube; this indicates that surface pinning plays an important role when placing these samples in a sample cell. In a columnar model for the structure, this would correspond to having the column axes parallel to the long axis of the tube, while in a smectic model it would correspond to preferential orientation of the layers parallel to the capillary walls. Rotating the capillary tube around the long axis did not indicate any preferential alignment.

If we assume that surface alignment and strain induced by the glass interface persists a macroscopic distance into the sample, possibly affecting transition temperatures, then clearly such effects would be more pronounced in experimental configurations (such as thin capillary tubes) incorporating a large surface-to-volume ratio. Surface interactions may also account for the differences seen in transition temperatures measured in DSC vs X-ray diffraction.

Hexacyclen **2e**, the homologue of **2a** with one fewer CH_2 group per tail, also displayed mesophase behavior and was studied in detail. The DSC first heating scan revealed a broad peak centered

(13) Safinya, C. R.; Clark, N. A.; Liang, K. S.; Varady, W. A.; Chiang, L. Y. *Mol. Cryst. Liq. Cryst.* **1985**, *123*, 205–216.
(14) Fontes, E.; Heiney, P. A.; Ohba, M.; Haseltine, J. N.; Smith, A. B., III *Phys. Rev. A* **1988**, *37*, 1329–1334.
(15) Fontes, E.; Heiney, P. A.; Haseltine, J. N.; Smith, A. B., III *J. Phys. (Paris)* **1986**, *47*, 1533–1539.

at 58 °C, a doublet at 106 °C, and another doublet at 142 °C. The second heating, performed after waiting 30 min, revealed only a single peak at 141 °C. X-ray diffraction measurements indicate a transition from the isotropic phase to a mesophase resembling that of **2a** at 144 ± 3 °C. When the sample was cooled from 125 °C to room temperature, followed by a 24-h wait, a diffraction pattern characteristic of a crystal was observed. The heat capacity peak corresponding to the crystal–mesophase transition was not seen on the second DSC scan, but it is possible that the sample was supercooled in the mesophase after the first DSC scan or formed a glass phase. TGA on **2e** indicated the presence of a small quantity of methanol.

5. Other Compounds

As indicated in Scheme I, a number of other hexasubstituted azacrown molecules were studied, none of which exhibited a liquid crystalline mesophase. Many of those were difficult to study as they tended to form nonequilibrium crystal structures on cooling, depending on the cooling rate. All DSC temperatures in this section are taken from the second heating of the sample.

Hexacyclen **2b** is similar to **2a** and **2e** except for a considerably shorter tail length. X-ray diffraction studies on cooling indicate a transition between the isotropic phase and a glass–crystal coexistence region at 125 °C. DSC measurements display a slope change at 130 °C, in reasonable agreement with the transition seen in the X-rays, and a sharp peak at 177 °C, indicating a transition not seen in the X-rays. Optical microscopy studies indicate that on first heating, a phase appears at 130 °C that consists of small crystallites formed on the surface of the glass slide and cover slip together with isotropic fluid between the slides. The sample enters the isotropic phase at 175 °C and can then be cooled to a room temperature glass. Both DSC and optical microscopy indicated the same transitions, since both require small amounts of sample that are in close contact with a surface of a sample cell, while the X-ray experiments tend to measure more of the bulk sample. Hexacyclen **2c**, which has no aliphatic tail, goes directly from the isotropic phase into a glassy room temperature phase. It has a previously reported[9] melting point of 157–161 °C.

If we then change the linkage between the core and the aromatic ring by reducing the carbonyl to a methylene unit, as in **3a**, both DSC and X-rays indicate a crystal-to-isotropic transition at 73 °C. By shortening the tail to produce **3b**, DSC indicates a transition at 81 °C, while X-rays indicate a crystal–isotropic transition between 25 and 61 °C. Optical microscopy gives transition temperatures of 64, 72, or 84 °C, depending on the thermal history. In **3c**, where the tail is removed altogether, we observe a crystal–isotropic transition at 74 °C from X-ray diffraction, while the DSC indicates a transition at 118 °C, in agreement with the previously reported[10] value of 120–121 °C.

In **2d**, where the aromatic group was replaced by five methylene units to link the core with the long aliphatic tail, a crystal–isotropic transition at 92 °C was observed. DSC measurements indicate that nonequilibrium crystal structures can also be present in this sample. Shortening the tail as in **2f** gives a crystal–isotropic transition at 96 °C as indicated by X-ray diffraction, while both DSC and optical microscopy indicate a wealth of nonequilibrium phases. Finally, removal of all heteroatoms in the side chains results in **3d**, a compound that displays a crystal–isotropic transition at 42 °C.

6. Computer Simulations

To gain further insight into the microscopic structure of the mesophase, we performed energy-minimization calculations to determine the optimal conformation of the isolated molecule **2a**. The calculations were carried out with the MacroModel program,[16] which employs a modification of Allinger's MM2 molecular mechanics force field.[17] The minimization scheme chosen was the default block diagonal Newton Raphson method with terminal-atom movement. The convergence criterion for the simulations was that the rms gradient of the molecular energy be less than 0.01 kJ/Å·mol.

A first guess for the conformation, based on the chemical formula, would be that the molecule is essentially planar with tails radiating out symmetrically to form a 6-fold structure. We quickly found, however, that a planar conformation for the inner-core ring is highly unfavorable. The core tends to adopt a more buckled chair conformation, whereas the overall molecule remains relatively flat with the tails tending to lie essentially in the same plane. Figure 3a shows an approximately 6-fold conformation for the molecule with enlarged top and side views of the core conformation. The energy of this conformation is calculated to be approximately 600 kJ/mol with an rms gradient of 0.62 kJ/Å·mol.

Further study, however, shows that van der Waals interactions between the tails cause them to group together. Figure 3b shows a conformation in which the tails pair up to form an approximately 3-fold structure. The energy of such a conformation is typically found to be between 515 and 580 kJ/mol with an rms gradient of 0.50 kJ/Å·mol. The tail–tail interaction is further enhanced if the tails cluster in groups of three to form an essentially linear molecule, as shown in Figure 3c. In this case we calculate a conformation energy of approximately 400 kJ/mol with an rms gradient of 0.01 kJ/Å·mol, significantly lower than that of the 6-fold and 3-fold conformations. In all cases, we find that the end-to-end distance of the molecule along its longest direction is on the order of 50 Å.

As observed previously by Tatarsky et al.,[6] the open area remaining inside the core is quite small. Examination of the enlarged views of the core rings in each of the conformations shows that in all cases the ring maintains a folded conformation with a small and asymmetric center cavity of ca. 0.8–1.5 Å (as measured from van der Waals radii). This implies that the inner volume of putative "tubes" must be quite small.

It must be emphasized that the above simulations were performed on individual, isolated molecules in a hypothetical motionless state.[18] In a condensed phase, intermolecular interactions will play a crucial role in determining intramolecular conformations. Therefore, such simulations should be considered only as useful guides to condensed-phase structures. Our calculations do, however, show that tail–tail correlations play an important role in determining the molecular shape, which in the isolated molecule would appear to be linear.

7. Discussion

The X-ray diffraction experiments and computer simulations presented above indicate that a layered smectic A or C structure may be a viable alternative to a columnar discotic structure for **2a** and **2e**. We now discuss the relative merits of these two models.

The primary arguments in favor of a columnar structure are as follows. (1) The structure of the molecule possesses intrinsic 6-fold symmetry, and hence the most symmetric way to organize fully stretched molecules is in a columnar structure. (2) The shearing and homeotropic orientation measurements of Lehn et al. were reported to be consistent with a columnar structure but inconsistent with a layered structure.[3] (3) The d spacing of the strong low-q X-ray diffraction peak is $2\pi/q$ = 32.6 Å. In a hexagonal structure, this is reduced by $2/\sqrt{3}$ from the nearest-neighbor distance, which is therefore ca. 37.7 Å. The layers in a smectic structure, on the other hand, would have to be 32 Å thick, considerably thinner than the length of one molecule. This suggests that the hexagonal columnar structure is mildly favored over the smectic as less interpenetration is required between adjacent molecules.

In response to these arguments, we note the following. (1) The molecules themselves are quite flexible, and in fact the energy-minimized structure of an isolated molecule does *not* appear either

(16) Still, W. C.; Mohamadi, F.; Richards, N. G. J.; Guida, W. C.; Lipton, M.; Liskamp, R.; Chang, G.; Hendrickson, T.; Degunst, F.; Hasel, W. MacroModel V2.5, Department of Chemistry, Columbia University, New York, NY 10027.

(17) Allinger, N. *J. Am. Chem. Soc.* **1977**, *99*, 8127–8134.

(18) Engler, E. M.; Andose, J. D.; Schleyer, P. von R. *J. Am. Chem. Soc.* **1973**, *95*, 8005–8025.

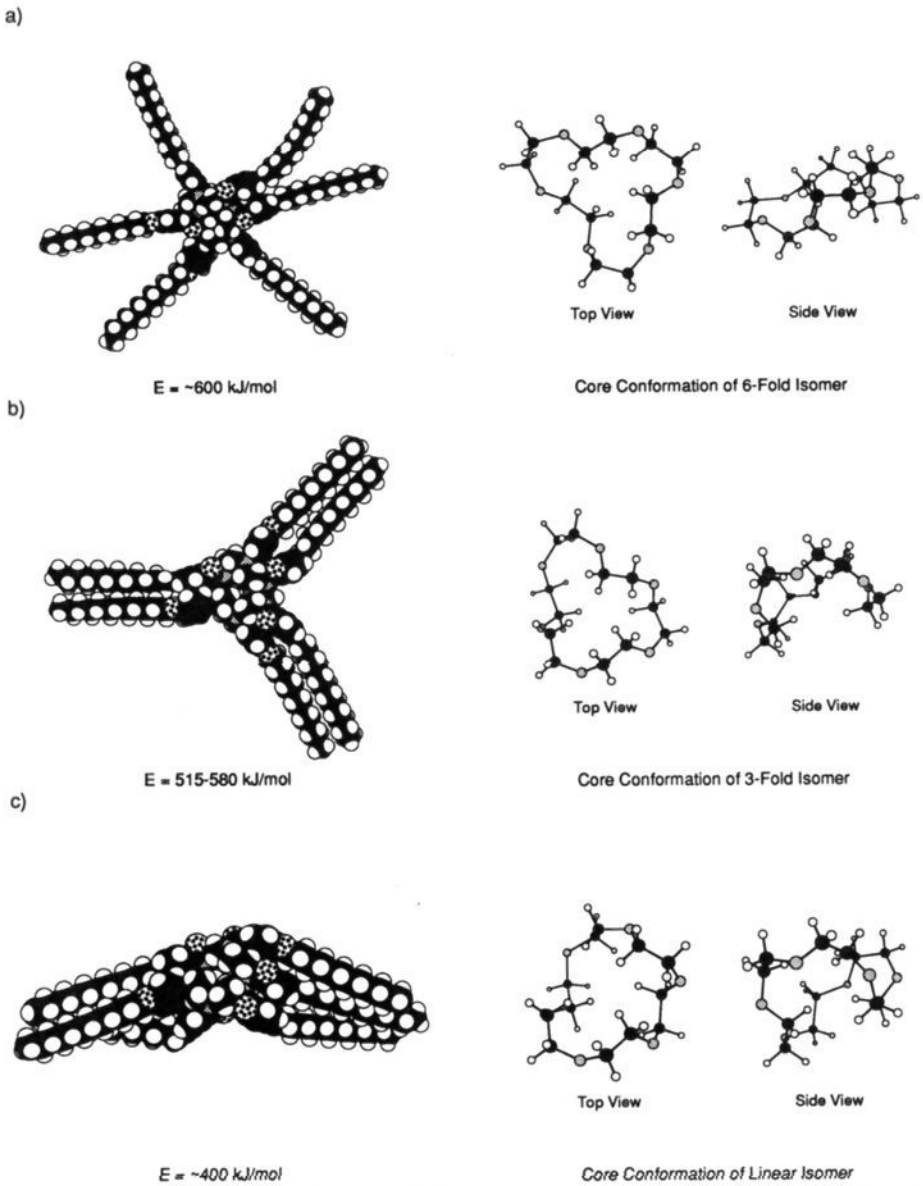

Figure 3. Results of computer simulations of **2a**, showing both space-filling models of the entire molecule and ball-and-stick models of the central core. (a) and (b) display the higher energy disclike conformations, while (c) displays the lowest energy rodlike conformation. Note that in none of the conformations shown is there any significant empty space in the core, which instead of adopting a circular, planar conformation prefers to adopt an asymmetric, nonplanar form with very little empty volume in the center.

to be planar or to possess pseudo 6-fold symmetry. (2) Our observation of orientation in a thin capillary tube is consistent with the shearing experiments of Lehn et al.; however, they can also be explained by assuming that smectic *layers* (rather than molecules) are aligned along the glass surface and along the shearing direction. (3) It is true that a postulated smectic structure would either have to be S_C with a large tilt angle or else S_A with a high degree of interpenetration of layers; in fact, a columnar structure also requires a fair degree of interpenetration, since the end-to-end length of the molecule along its longest direction is on the order of 50 Å, independent of the detailed conformation.

The principal arguments for a smectic structure are as follows. (1) There is no direct evidence, from X-ray diffraction or other measurements, of 6-fold or even centered rectangular point symmetry in the mesophase structure, as might be measured for example by rotating the sample with the X-ray detector set at the Bragg angle.[19] (2) More important, the higher order diffraction peaks expected for a columnar structure are completely missing. (3) Energy-minimization calculations indicate a preference for linear, rather than planar, molecular conformation.

Point 2 requires some amplification. Diffraction experiments of course measure the square of the Fourier transform of the electronic charge; the observation of only a single peak implies that the average electron density is nearly sinusoidal. Higher order peaks in liquid crystal smectic structures are generally found to be weak or absent. It is generally considered that the absence of these peaks corresponds to some combination of layer fluctuations, molecular permeation from layer to layer, and molecular structure factor. However, in columnar structures the columns are typically better defined than the smectic layers, resulting in (110) and (200) diffraction peaks that are only reduced by ~2 orders of magnitude from the (100). We have used the linear and 6-fold structures obtained from our energy-minimization calculations to compute static molecular structure factors and find that the wave vector dependence of these structure factors is comparable to that of more traditional molecules. Thus, the absence of higher order peaks cannot be rationalized simply on the basis of static molecular structure factors.

(19) This is of course really an argument *against* a columnar structure and could be eliminated by even a single observation of a sharp 6-fold diffraction pattern.

We find several possible explanations for the absence of higher order peaks. One is that the structure is columnar but incorporates very large lattice fluctuations[3] (with rms motions on the order of a column thickness). A second possibility is that the columns are well-defined but that there is a high degree of intramolecular thermal motion, resulting in an almost sinusoidal charge distribution within one column. In this case, the rationale for forming a columnar structure in the first place is less clear. Finally, the molecules may be essentially linear and organized in layers, with permeation and layer fluctuations as discussed above.

Mertesdorf and Ringsdorf[20] have recently studied a closely related cinnamoyl-substituted hexacyclen. On the basis of d spacings observed in powder X-ray diffraction, as well as optical microscopy observations, they conclude that those compounds form columnar phases. To our knowledge, no measurements on *any* aza derivative has conclusively proved the existence of hexagonal structure (as manifested for example by (110) X-ray diffraction peaks or a 6-fold single-crystal X-ray pattern). Nevertheless, at the present time the preponderance of evidence for the cinnamoyl derivative indicates a columnar structure, while for **2a** a smectic phase is weakly preferred.

(20) Mertesdorf, C.; Ringsdorf, H. Private communication.

Acknowledgment. We would like to thank E. Fontes, G. Furst, S. Kycia, A. G. McGhie, G. Rosenbaum, and G. Vaughan for their expert assistance. We also acknowledge useful conversations with R. Shashidhar and S. Pfeiffer. This work was supported by the National Science Foundation, Grant No. DMR 89-01219. Additional support was provided by the National Science Foundation, MRL Program, Grant No. DMR-8819885. Portions of this research were carried out on Beamline X9-A of the National Synchrotron Light Source, Brookhaven National Laboratory. Biostructures PRT Beamline X9-A is supported by NIH RR01633. Brookhaven National Laboratory is supported by the United States Department of Energy, Division of Materials Sciences and Division of Chemical Sciences.

Singlet Oxygen and Electron-Transfer Mechanisms in the Dicyanoanthracene-Sensitized Photooxidation of 2,3-Diphenyl-1,4-dioxene

Scott K. Silverman and Christopher S. Foote*

Contribution from the Department of Chemistry and Biochemistry, University of California, Los Angeles, Los Angeles, California 90024-1569. *Received April 8, 1991*

Abstract: The 9,10-dicyanoanthracene-sensitized photooxidation of 2,3-diphenyl-1,4-dioxene in CH_3CN produces ethylene glycol dibenzoate and small amounts of epoxide. Most of the diester is formed from singlet oxygen via the dioxetane, and only a small amount by electron transfer. The epoxide is a primary electron-transfer product. Various mechanistic possibilites for the electron-transfer process are considered.

Schaap reported that the 9,10-dicyanoanthracene (DCA)-sensitized photooxidation of 2,3-diphenyl-1,4-dioxene (DPD) in acetonitrile gives ethylene glycol dibenzoate (EGDB) as the only isolable product (Scheme I).[1] It was assumed that this product is formed by electron transfer, which produces analogous cleavage products from aromatic alkenes with DCA.[2,3] However, singlet oxygen can also be formed in large quantities in this reaction,[4-6] and it has been suggested that singlet oxygen reacts with DPD to give the dioxetane precursor of EGDB.[7] We have reinvestigated the DCA-sensitized photooxidation of DPD to determine whether singlet oxygen, electron transfer, or a combination is responsible for the observed products.

Scheme I

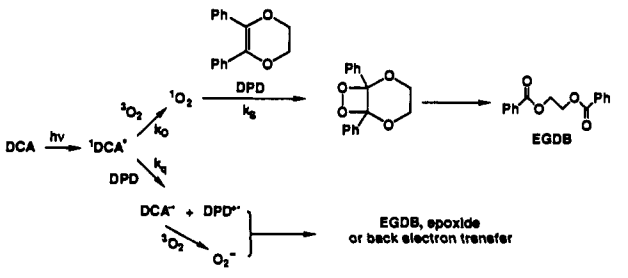

Results

As reported by Schaap, DCA-sensitized photooxidation of DPD in acetonitrile at varying DPD concentrations at 25 °C leads to EGDB as the major isolable product. When the reaction is followed by ^{1}H NMR, an intermediate, shown to be DPD dioxetane, is formed; the dioxetane decomposes completely to EGDB upon heating for 2 h at 60 °C. A minor product in the reaction is also observed, shown to be the unstable 2,3-diphenyl-1,4-dioxene oxide, as discussed below. Reaction of DPD with singlet oxygen generated from polymer-bound Rose Bengal in methylene chloride[8] gives EGDB as the major product, also via the dioxetane, as determined by ^{1}H NMR. The epoxide is nearly undetectable in this reaction.

If the singlet oxygen route to EGDB predominates in the DCA-sensitized reaction, product formation should be inhibited

(1) Schaap, A. P.; Zaklika, K. A.; Kaskar, B.; Fung, W.-M. *J. Am. Chem. Soc.* **1980**, *102*, 389-391.
(2) Eriksen, J.; Foote, C. S. *J. Am. Chem. Soc.* **1980**, *102*, 6083-6088.
(3) Gould, I. R.; Ege, D.; Moser, J. E.; Farid, S. *J. Am. Chem. Soc.* **1990**, *112*, 4290-4301.
(4) Dobrowolski, D. C.; Ogilby, P. R.; Foote, C. S. *J. Phys. Chem.* **1983**, *87*, 2261-2263.
(5) Foote, C. S. *Tetrahedron* **1985**, *41*, 2221-2227.
(6) Kanner, R. C.; Foote, C. S. *J. Am. Chem. Soc.* **1991**, in press.
(7) Spada, L. T.; Foote, C. S. *J. Am. Chem. Soc.* **1980**, *102*, 391-393.
(8) Schaap, A. P.; Thayer, A. L.; Blossey, E. C.; Neckers, D. C. *J. Am. Chem. Soc.* **1975**, *97*, 3741-3745.

0002-7863/91/1513-7672$02.50/0